THE JOURNAL OF PHYSICAL CHEMISTRY B

Article

pubs.acs.org/JPCB

Computational Studies of Protonated β-D-Galactose and Its Hydrated Complex: Structures, Interactions, Proton Transfer Dynamics, and Spectroscopy

Hong-bin Xie,*[,†,‡] Lin Jin,[‡] Svemir Rudić,[§] John P. Simons,[§] and R. Benny Gerber*[,‡,∥]

[†]Key Laboratory of Industrial Ecology and Environmental Engineering (MOE), School of Environmental Science and Technology, Dalian University of Technology, Dalian 116024, China

[‡]Department of Chemistry, University of California, Irvine, California 92697-2025, United States

[§]Department of Chemistry, Physical and Theoretical Chemistry Laboratory, Oxford University, South Parks Road, Oxford OX1 3QZ, U.K.

[∥]Institute of Chemistry and The Fritz Haber Research Center, The Hebrew University, Jerusalem 91904, Israel

Supporting Information

ABSTRACT: We present an exploration of proton transfer dynamics in a monosaccharide, based upon ab initio molecular dynamic (AIMD) simulations, conducted "on-the-fly", in β-D-galactose-H^+ (β-Gal-H^+) and its singly hydrated complex, β-Gal-H^+-H_2O. Prior structural calculations identify O6 as the preferred protonation site for O-methyl α-D-galactopyranoside, but the β-anomeric configuration favors the inversion of the pyranose ring from the $^4C_1$ chair configuration, to $^1C_4$, and the formation of proton bridges to the (axial) O1 and O3 sites. In the hydrated complex, however, the proton bonds to the water molecule inserted between the O6 and Ow sites, and the ring retains its original $^4C_1$ conformation, supported by a circular network of co-operatively linked hydrogen bonds. Two distinct proton transfer processes, operating over a time scale of 10 ps, have been identified in β-Gal-H^+ at 500 K. One of them leads to chemical reaction and the formation of an oxacarbenium ion (accompanied by the loss of an H_2O molecule). In the hydrated complex, β-Gal-H^+-H_2O, this reaction is suppressed, and the proton transfer, which involves multiple jumps between the sugar and the H_2O, creates an H_3O^+ ion, relevant, perhaps, to the reactivity of protonated sugars both in the gas and condensed phases. Anticipating future spectroscopic investigations, the vibrational spectra of β-Gal-H^+ and β-Gal-H^+-H_2O have also been computed through AIMD simulations conducted at average temperatures of 300 and 40 K and also through vibrational self-consistent field (VSCF) calculations at 0 K.

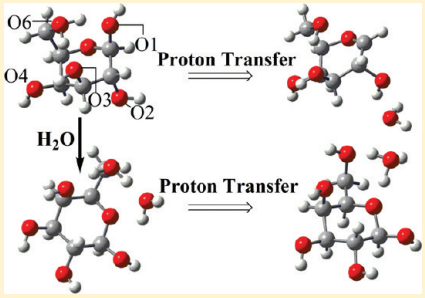

I. INTRODUCTION

The acid or enzyme-catalyzed hydrolysis of sugars begins with protonation,[1] providing the critical first step in the cleavage or formation of the glycosidic linkage. Glycosidase enzymes are involved in a host of biological[2] as well as industrial processes and in the context of biofuel production, enzymes (as well as acids) are used as catalysts for the hydrolysis reaction that converts complex polysaccharides in raw feedstock to simple sugars, a context that has prompted numerous experimental and ab initio molecular dynamic (AIMD) simulations of sugar-degradation mechanisms in acidic media.[3−5] Theoretical studies of sugar-degradation mechanisms in aqueous solution have indicated the important role played by H_2O, which may change the reaction pathway[5] or block the reaction due to competition for the proton.[4]

A recent experimental and computational investigation of a protonated sugar, *O*-methyl α-D-galactopyranoside, conducted in the gas phase,[6] has revealed proton-bound structures that bridge neighboring pairs of oxygen atoms, preferentially O6 and O4 (see Scheme 1). Protonation at the glycosidic site, O1, although far less favored energetically, resulted in fragmentation

Scheme 1

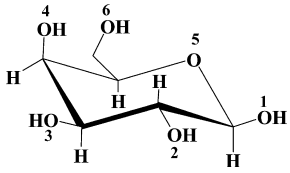

to create an oxacarbenium ion, which resembled the transition state structure in the proposed mechanisms of acid-catalyzed hydrolysis.[1,2] Moving from structure to dynamics, we now present an exploration of the proton transfer dynamics, based upon AIMD simulations conducted "on-the-fly", in β-D-galactose-H^+ (β-Gal-H^+) and its singly hydrated complex, β-Gal-H^+-H_2O in the gas phase, to provide a microscopic framework where interactions and structural dynamics can be

Received: March 25, 2012
Revised: March 31, 2012
Published: April 10, 2012

examined in detail, at an adequate level of theory. Anticipating future spectroscopic investigations, and following a strategy first reported by Iyengar et al.,[7] the vibrational spectra of βGal-H$^+$ and βGal-H$^+$-H$_2$O have also been computed, through AIMD simulations at 300 K. For spectra at low temperatures, we carried out vibrational self-consistent field (VSCF) calculations, which are for 0 K, and also AIMD simulations at 40 K. The accuracy of the VSCF method has already been successfully demonstrated for a range of carbohydrates.[8−10]

There is extensive literature on MD modeling of sugars employing empirical force fields, e.g., Amber, Charmm, and OPLS,[11−14] but such force fields in their standard version cannot properly describe chemical processes, such as proton transfer, and although dynamics simulations using semi-empirical electronic structure methods, such as PM3, have been used successfully to simulate systems such as photo-ionized amino-acids or their proton-bound dimers,[15−17] their validity for saccharides has not been established. On the other hand, several studies of dynamical processes in small saccharides and their hydrated complexes have been conducted through AIMD simulations using density functional theory (DFT) potentials, based on BLYP or better, dispersion-corrected, BLYP-D functionals.[8,9,18] These are known to be capable of describing proton transfer processes[19−21] and extensive simulations of such dynamics have been reported by Gaigeot and co-workers for protonated peptides and proton-bound complexes of amino acids.[22]

Accordingly, this approach is employed here to explore the equilibrium structures, proton transfer processes and structural transitions in the protonated β-D-galactose systems. We also present calculations of their vibrational spectroscopy, both for the cold protonated systems in the gas phase, and at temperatures at which proton-transfer processes take place, since vibrational spectroscopy will be the prime tool for their future experimental exploration.[6]

II. THEORETICAL METHODS

2.1. Global Minimum Search. Two alternative strategies were employed. In the first, the seven lowest energy conformers reported by Momany et al.[23] were adopted to model the initial structure of β-D-galactose-H$^+$, and the proton was added to each of the six sites, O1−O6, identified in Scheme 1. These structures were then optimized through ab initio calculations conducted at the MP2/DZV level, using the GAMESS program suite,[24] providing a set of 42 geometries and relative energies from which a global minimum structure could be identified; their harmonic vibrational frequencies were also calculated at the HF/DZV level. Calculations conducted at the MP2/DZP and spin-coupled SOS-RIMP2/def2-TZVP levels were used to confirm the global minimum assignment.

The βGal-H$^+$-H$_2$O system was modeled similarly, by adding the H$_2$O molecule to each of the six identified sites in the two lowest energy isomers of βGal-H$^+$, followed by their ab initio optimization at the MP2/DZV level.

The alternative analysis began with a series of unrestricted surveys of the large number of possible protonated structures generated through a molecular mechanics conformational search, using the mixed Monte Carlo multiple minimization and large scale low mode method, as implemented in the MacroModel software[25] (Schrödinger). The low energy conformers as well as a number of relevant higher energy structures were then submitted for geometry optimization using the Gaussian 03 suite of programs[26] and DFT at the B3LYP/6-311++G(d,p) level. More accurate single point energies, calculated at the MP2/6-311++G(d,p) level of theory, were corrected for zero point energy (ZPE) using the DFT harmonic frequencies to provide a final set of relative energies, molecular structures, and vibrational frequencies. Similar procedures were adopted for the hydrated complex.

In all cases, the lowest energy structures identified through the alternative schemes were found to be the same.

2.2. Ab Initio Molecular Dynamics Calculations. AIMD calculations were conducted using the dispersion corrected[27,28] DFT BLYP-D functional along with a triple-ξ valence polarized basis set (TZVP) within the resolution-of-the-identity (RI)[29] approximation. The global minima of βGal-H$^+$ and βGal-H$^+$-H$_2$O, obtained at the MP2/DZP level, were taken as the initial structures and the simulations were performed at 300 and 500 K using the Nosé−Hoover thermostat[30,31] to maintain the temperature of the system; the total duration of each simulation was 9.675 ps (20000 time steps). Calculations were conducted using the TURBOMOLE package.[32] To study how the charge distribution changes in the simulation, atomic charges based on natural bond orbital (NBO)[33] analysis were also calculated along the trajectories of the AIMD simulations.

2.3. VSCF Algorithms. Anharmonic vibrational frequency calculations were conducted using the VSCF method, implemented in the GAMESS program suite.[24] Second-order perturbation theory, which has been used to correct the standard VSCF approximation[34] (the VSCF-PT2 method) was also applied in the present work using a scaled Hartree−Fock potential. It was obtained by first comparing the harmonic frequencies calculated at the HF/DZV level with those calculated at the MP2/DZP level to create the scaling factors λ_i for each normal mode (assuming the modes were similar)

$$\lambda_i = \omega_i^{\mathrm{MP2}}/\omega_i^{\mathrm{HF}} \tag{2.1}$$

and then employing them to generate an adapted HF surface given by

$$V_{\mathrm{HF}}^{\mathrm{scaled}}(Q_1, ..., Q_N) = V_{\mathrm{HF}}^{\mathrm{standard}}(\lambda_1 Q_1, ..., \lambda_N Q_N) \tag{2.2}$$

where $V_{\mathrm{HF}}^{\mathrm{standard}}$ is the standard HF potential.

The method, which has been fully described elsewhere,[10,35−42] has now been applied to a number of biological molecules, including carbohydrates and their hydrated complexes,[8−10] and found to give results in good accord with experimental measurements conducted at low temperatures in the gas phase.

2.4. "On-the-Fly" Dynamics Computation of Vibrational Spectra. The calculation of vibrational spectroscopy from ab initio MD has the advantage of applicability to nonzero temperature. The classical approximation on the other hand neglects quantum effects, which especially affect the accuracy of the predicted intensities. Within linear response theory, the infrared line shape function, $I(\omega)$, can be written as the Fourier transform of the dipole moment time correlation function:[43]

$$I(\omega) = \frac{2\pi\beta\omega^2}{3cV}\int_{-\infty}^{\infty} \mathrm{d}t\langle M(t)\cdot M(0)\rangle \exp(i\omega t) \tag{2.3}$$

where $\beta = 1/kT$, c is the speed of light in vacuum, V is the volume, the angular brackets indicate a statistical average of the autocorrelation of the dipole moment M of the system, and the quantum correction factor, of the form $\beta\hbar/(1 - \exp(\beta\hbar\omega)$ has been taken into account. In the present work, the dipole moment $M(t)$ of system was calculated by "on-the-fly"

dx.doi.org/10.1021/jp3028325 | J. Phys. Chem. B 2012, 116, 4851−4859

dynamics simulations using the CP2K/QUICKSTEP package[44] and the BLYP-D functional[45] (corrected for dispersion), the double-ζ valence polarization (DZVP) basis set, and the Goedeker, Teter, and Hutter (GTH)-type pseudo potential.[46] The one-electron orbitals were expanded in a plane-wave basis set, with a kinetic energy cutoff of 300 Ry. The AIMD simulations were initialized at the global energy configuration of the system. A strict NVE ensemble was used with time step 0.5 fs and simulations were carried out at average temperatures of ~300 K and ~500 K. The Berry phase representation[47] in the modern theory of polarization was used to calculate the dipole moment of the box cell. The system dipole moment was collected at each time step over a cubic unit cell of side dimension 27 Å along 10 ps trajectories for each simulation. To generate better statistics, ten 10 ps trajectories were run for each system; particle momenta were sampled from the Maxwell distribution at the inverse temperature. The final IR spectrum was obtained by averaging the ten corresponding $I(\omega)$ functions. The assignment of spectral bands to individual atomic modes of motion was performed by matching the Fourier transform of the time dependence of the bond length formed by selected groups of atoms, to corresponding IR bands.

III. RESULTS AND DISCUSSION

3.1. Conformational Structures. The predicted lowest energy structures of the carbohydrate ion, βGal-H$^+$, and its hydrated complex, βGal-H$^+$-H$_2$O, are shown in Figures 1 and 2; Table 1 lists their relative energies, calculated at the MP2/DZV level and also the BLYP-D/TZVP level. In contrast to the neutral carbohydrate, where the pyranose ring presents a $^4C_1$ chair conformation (shown in Scheme 1) in its minimum energy configuration, protonation of βGal creates an inverted, $^1C_4$ conformer, which switches the axial/equatorial orientations around the ring to facilitate proton bridging from the preferred protonation site, O6, to the (axial) O3 and (axial) O1 sites (see Figure 1).

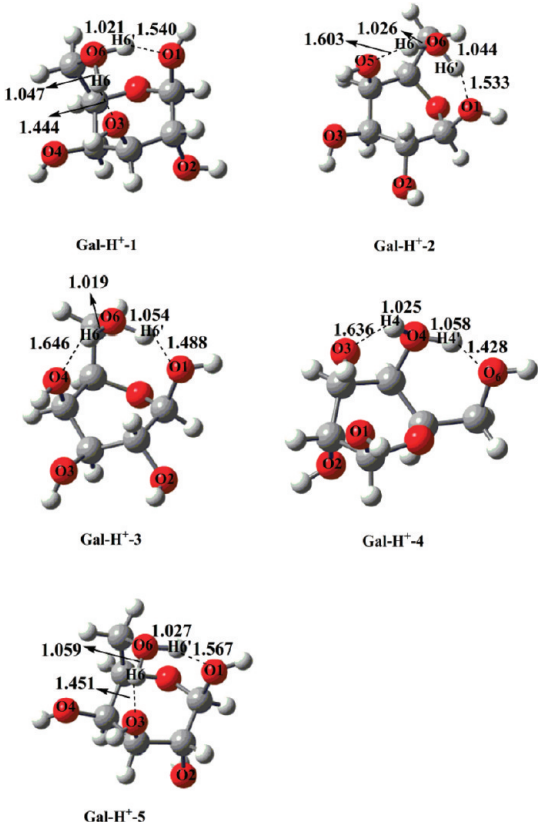

Figure 1. Structures of the lowest energy conformers of β-D-galactose-H$^+$ calculated at the MP2/DZV level. Relative energies are listed in Table 1.

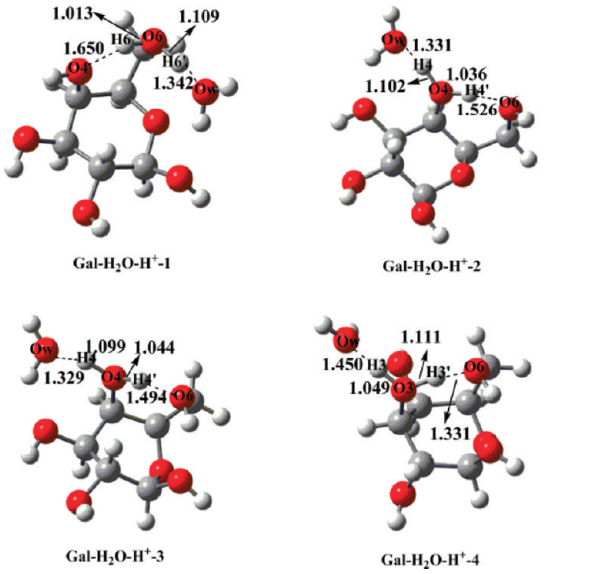

Figure 2. Structures of the lowest energy conformers of β-D-galactose-H$^+$-H$_2$O calculated at the MP2/DZV level. Relative energies are listed in Table 1.

Table 1. The Relative Energies (kcal/mol) of the Lowest Energy Conformers of β-D-Galactose-H$^+$ and β-D-Galactose-H$^+$-H$_2$O, Calculated at the MP2/DZV and BLYP-D/def2-TZVP (*Italic*) Levels, and Their Corresponding Relative ZPEs (In Brackets) Calculated at the MP2/DZV Level

conformer	energy	conformer	energy
Gal-H$^+$-1	0.0; *0.0*(0.0)	Gal-H$^+$-H$_2$O-1	0.0; *0.0*(0.0)
Gal-H$^+$-2	1.1; *3.2*(0.5)	Gal-H$^+$-H$_2$O-2	1.3; *2.1*(−1.2)
Gal-H$^+$-3	1.3; *3.7*(0.3)	Gal-H$^+$-H$_2$O-3	3.2; *1.2*(−1.0)
Gal-H$^+$-4	2.0; *6.7*(0.0)	Gal-H$^+$-H$_2$O-4	3.6; *3.6*(−0.3)
Gal-H$^+$-5	3.6; *1.5*(−0.1)	Gal-H$^+$-H$_2$O-5	3.7; *0.1*(−0.8)

The hydrated complex behaves quite differently. In contrast to βGal-H$^+$, where movement of the two shared atoms, O6 and O3, or O6 and O1 for that matter, is highly restricted (since they are bound into the molecular scaffold), the proton is now shared with Ow. This is facilitated by the freedom of the water molecule to move into the most favorable site, and it forms a proton-bound dimer linked to O6 with an O6−H$^{\delta+}$−Ow angle of 180°, while the pyranose ring reverts to its original $^4C_1$ conformation (see Figure 2). The hydrogen bonded network also changes: with O4 now axially rather than equatorially oriented, a "partial" proton bridge also links the O6 and O4 sites, and the positive charge is shared across the [O4···H-(O6)H···Ow]$^+$ unit, enabling the formation of an extended, co-operatively linked hydrogen-bonded ring.

3.2. Proton Transfer Dynamics. In studying the dynamics of the βGal-H$^+$ and βGal-H$^+$-H$_2$O systems, it is not feasible to use the MP2 potential (or other potentials of higher level) in view of the computational cost, and the cost-efficient potential

dx.doi.org/10.1021/jp3028325 | J. Phys. Chem. B 2012, 116, 4851−4859

BLYP-D was used instead, after testing its accuracy by comparing the BLYP-D and MP2/DZV methods for the energetics of the βGal-H$^+$ and βGal-H$^+$-H$_2$O conformers. The comparisons are shown in Table 1. Although there are a few exceptions, e.g., conformer **5** for βGal-H$^+$ and conformer **4** for βGal-H$^+$-H$_2$O, the energy rankings predicted by BLYP-D/def2-TZVP and MP2/DZV are comparable; despite the possible quantitative limitations of the BLYP-D potential,[48] it should be adequate for providing qualitative dynamical predictions.

β-D-Galactose-H$^+$. Representative snapshots along AIMD trajectories for βGal-H$^+$, starting from the global minimum conformation and calculated at 300 and 500 K, are presented in Figures 3 and 4, respectively. Proton (H6) transfer between O6

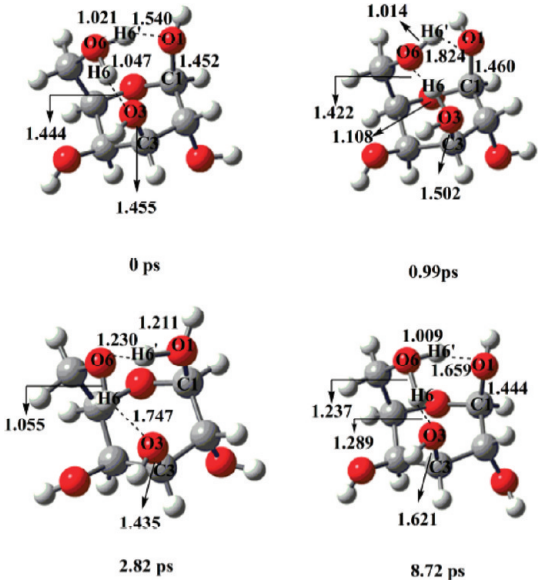

Figure 3. Representative snapshots and key interatomic distances (in Å) along AIMD trajectories of β-D-galactose-H$^+$, highlighting the proton motion at 300 K.

and O3 is predicted to occur with low probability at 300 K (see Figure 3; 0.987 ps), but at 500 K the (H6′) proton transfer to its neighboring O1 atom becomes the dominant process (see Supporting Information (SI)). [Similar motions occur in proton bound dimers, for example [H$_2$O−H$^+$−OH$_2$], where the proton undergoes large-amplitude motion (as large as 0.3 Å), even in its vibrational zero-point level.[49−55]] This transfer leads to rupture of the C1−O1 bond, the elimination of H$_2$O, and the initial formation of a [C$_6$H$_{11}$O$_5$]$^+$ ion, with an oxacarbenium structure (Product 1), as shown in Figure 4 (at 4.06 ps, where the probability of H6′ proton transfer reaches 100%). After that time, the C1−O1 distance rapidly extends (see Figure 5) and the products, H$_2$O and [C$_6$H$_{11}$O$_5$]$^+$ cannot return to the reactants. The [C$_6$H$_{11}$O$_5$]$^+$ ion can also adopt an alternative bicyclic configuration (Product 2), incorporating a five-membered ring supported by bonding between O6 and C1.

An NBO charge analysis, performed during the AIMD simulation at 500 K, revealed the changes in the distribution of the positive charge during the reaction of βGal-H$^+$. Figure 5 displays the evolution of the charge on the H$_2$O (H6′O1H1) product and the [C$_6$H$_{11}$O$_5$] fragment as the bond lengths O6···H6′, O1···H6′, and C1···O1 change with time, together with snapshots taken before (0 ps), and after (9.64 ps) the reaction. Once the chemical reaction occurs (signaled by the

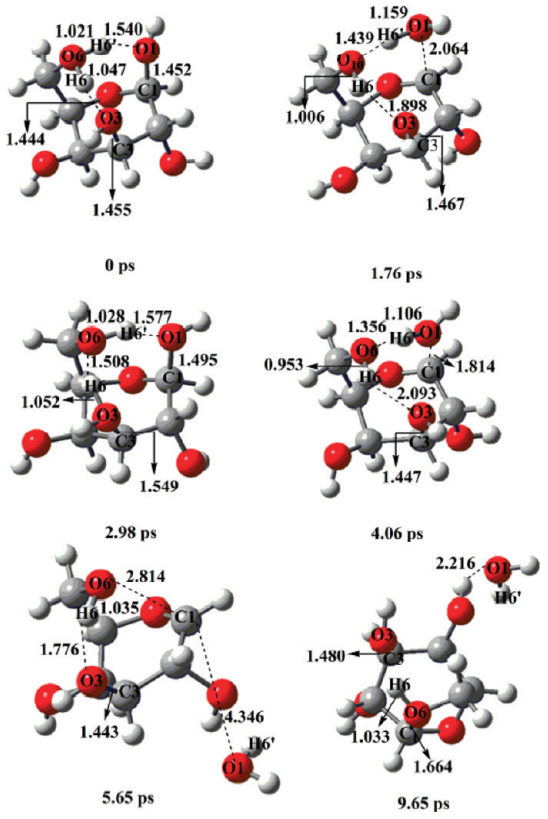

Figure 4. Representative snapshots and key interatomic distances (in Å) along AIMD trajectories of β-D-galactose-H$^+$, highlighting the proton motion at 500 K.

increase in the C1···O1 bond length beyond 4 Å, Figure 5), the positive charge on the water molecule decreases to near zero:

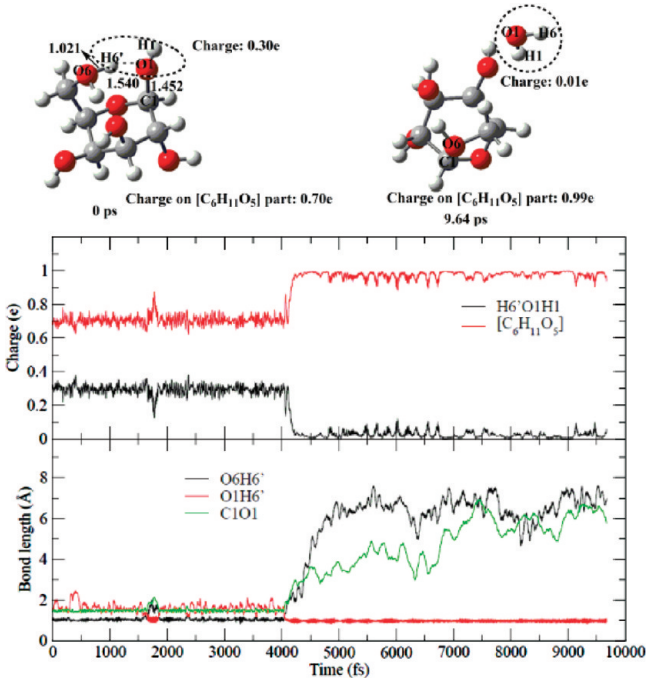

Figure 5. Evolution of the bond distances O6H6′, O1H6′, and C1O1, and the charges on the [H6′O1H1] and [C$_6$H$_{11}$O$_5$] units of β-D-galactose-H$^+$ at 500 K.

dx.doi.org/10.1021/jp3028325 | J. Phys. Chem. B 2012, 116, 4851−4859

the charge is almost completely transferred to the $[C_6H_{11}O_5]$ fragment. Its initial structure closely resembles that of the oxacarbenium intermediate (Product 1) postulated as the transition state in the acid (and enzyme) catalyzed hydrolysis of saccharides following protonation at the anomeric, O1 site.[1,2] It is also interesting to note how the positive charge is redistributed after the reaction. After the formation of the oxacarbenium ion, Product 1, C1 and O5 become more positive, while O2, O6, and O1 become more negative (see Figure 6), but when the bicyclic Product 2 is formed, O6 becomes more positive and O1 more negative.

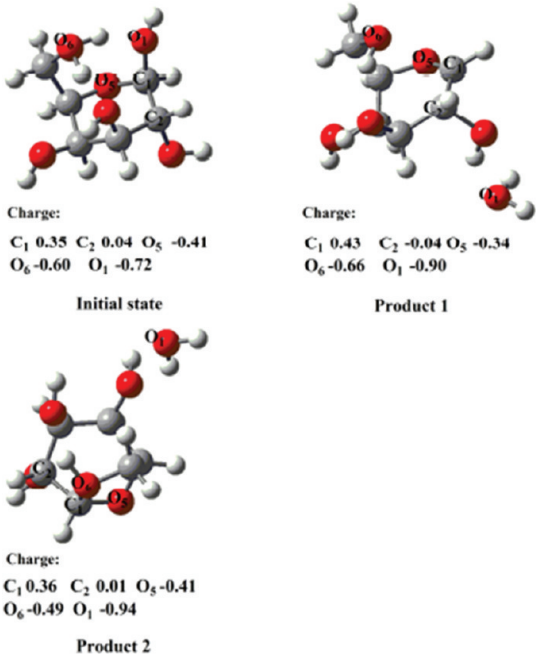

Figure 6. Natural atomic charges/e, that change significantly (by >0.07 e) in the reaction of β-D-galactose-H^+ at 500 K.

AIMD trajectories were also calculated starting from the second lowest energy conformer (**2**), predicted to adopt a boat-like, $B_{3,O}$ conformation supported by bridging across O6 and O4, and O6 and O1. The simulations predicted a similar reaction, again prompted by proton transfer from O6 to O1, even at 300 K.

β-D-Galactose-H^+-H_2O. Figures 7 and 8 show representative snapshots taken from AIMD simulations of βGal-H^+-H_2O, starting from the minimum energy conformation and conducted at 300 and 500 K. They reveal only one proton transfer path, even at 500 K, from O6 to the O_w atom on the bound water molecule, located between $(O6{-}H6')^{\delta+}$ and O1: the bound H_2O molecule competes with galactose for the proton, a result that recalls a previous MD simulation of protonated xylose and glucose in bulk, aqueous solution.[4,56] Since *intra*molecular proton transfer, leading to rupture of the C1−O1 bond, does not occur, instead of providing a conduit for proton transfer from O6 to O1, followed by the formation of an oxacarbenium ion, the bound water molecule actually *blocks* the reactive pathway.

The distribution of positive charge after proton transfer at 500 K, predicted through NBO calculations, is shown in Figure 9, which displays the evolution of the NBO charges on the $[H6'O_wH_wH_{wf}]$ and β-galactose units, and also the evolution of the bond lengths O6···H6′ and O_w···H6′. The positive charge

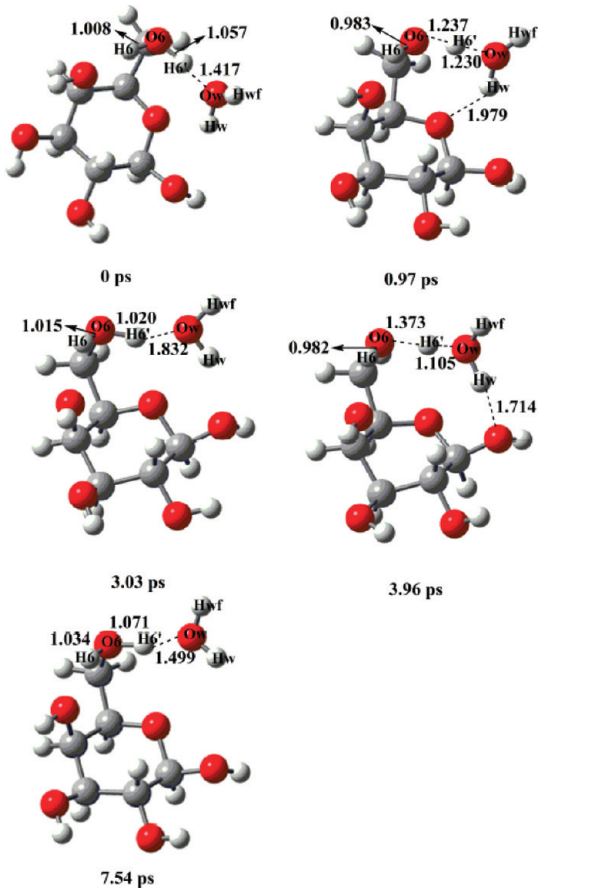

Figure 7. Representative snapshots and key interatomic distances (in Å) along AIMD trajectories of β-D-galactose-H^+-H_2O, highlighting the proton motion at 300 K.

moves from the sugar to the H_3O unit, reaching a maximum of 0.82 e at 4.44 ps, corresponding to a charge transfer of 0.18 e, compared with the initial distribution at 0 ps. A similar trend was found at 300 K.

3.3. Vibrational Spectroscopy. The focus here is on the OH vibrational modes since they reflect the shared proton interactions, and their experimental measurements will provide "reports" of the proton transfer dynamics between neighboring O atoms. Scheme 2 indicates the notation used to describe the OH stretch modes in βGal-H^+ and βGal-H^+-H_2O.

VSCF-PT2 Calculations. Tables 2 and 3 list the calculated wave numbers of the anharmonic and, for comparison, the corresponding harmonic OH vibrational stretch modes. Those that do not involve shared proton bonding, namely σ1−4, σw and σwf, all lie in the range 3590−3770 cm^{-1}, comparable to those in neutral sugars and their hydrated complexes.[57] By contrast, the VSCF predictions for the shared proton modes σ6 and σ6′ are very strongly displaced to 2004 cm^{-1} and 2680 cm^{-1}, respectively, in βGal-H^+, and 2888 cm^{-1} and 1464 cm^{-1} in βGal-H^+-H_2O. In addition there are very large differences between the harmonic (MP2/DZP) and anharmonic (VSCF-PT2) predictions for the mode σ6 in βGal-H^+, and σ6′ in βGal-H^+-H_2O, 473 cm^{-1} and 862 cm^{-1}, respectively, which implies a potential for the σ6 mode (in βGal-H^+) and the σ6′ mode (in βGal-H^+-H_2O) that is *too* anharmonic, causing a failure in the VSCF method.[58] Potentials of the two shared proton modes σ6 and σ6′, calculated at the HF/DZV level, presented in Figure 10, reveal a shoulder between 1.20 Å and 1.50 Å in βGal-H^+

dx.doi.org/10.1021/jp3028325 | J. Phys. Chem. B 2012, 116, 4851−4859

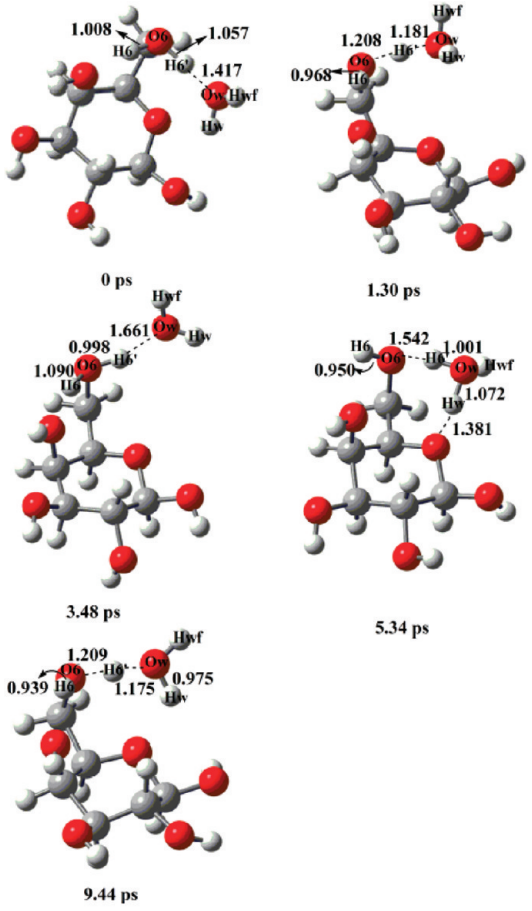

Figure 8. Representative snapshots and key interatomic distances (in Å) along AIMD trajectories of β-D-galactose-H^+-H_2O, highlighting the proton motion at 500 K.

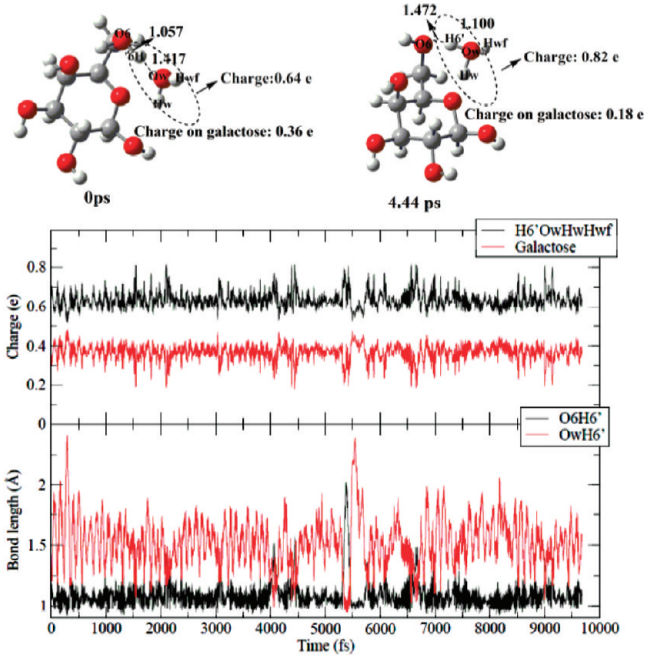

Figure 9. Evolution of the bond distances O6H6′ and OwH6′, and the charge on the [H6′OwHwHwf] unit of β-D-galactose-H^+-H_2O, at 500 K.

Scheme 2

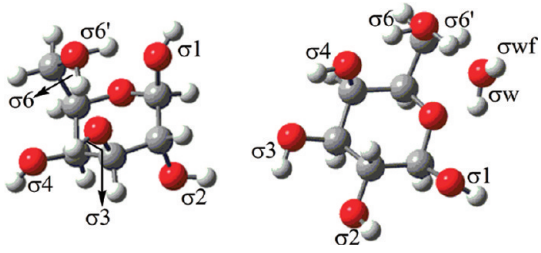

Table 2. Harmonic Wave Numbers/cm^{-1} and (Intensities/Debye^2/amu-Å^2) of OH bands of β-D-Galactose-H^+, Calculated at the HF/DZV and MP2/DZP Levels, and the Corresponding Anharmonic Calculations, Obtained by the VSCF-PT2 Method

	harmonic				VSCF-PT2	
mode	HF/DZV		MP2/DZP		scaled HF/DZV	
σ1	4065	(3.5)	3853	(3.3)	3668	(3.1)
σ2	4068	(4.1)	3897	(2.4)	3675	(3.6)
σ3	4084	(4.5)	3828	(3.3)	3651	(3.8)
σ4	4073	(2.5)	3904	(2.8)	3683	(2.3)
σ6	3105	(24.8)	2477	(33.1)	2004	(14.2)
σ6′	3531	(14.7)	2936	(24.1)	2680	(10.0)

Table 3. Harmonic Wave Numbers/cm^{-1} and (Intensities/Debye^2/amu-Å^2) of OH bands of β-D-Galactose-H^+-H_2O, Calculated at the HF/DZV and MP2/DZP Levels, and the Corresponding Anharmonic Calculations, Obtained by the VSCF-PT2 Method

	harmonic				VSCF	
mode	HF/DZV		MP2/DZP		scaled HF	
σ1	4065	(3.5)	3887	(2.6)	3665	(3.1)
σ2	4060	(2.2)	3883	(1.7)	3697	(1.9)
σ3	4052	(3.0)	3862	(2.3)	3673	(2.6)
σ4	4004	(4.2)	3796	(3.7)	3599	(3.7)
σ6	3623	(12.3)	3156	(14.5)	2888	(9.3)
σ6′	2531	(52.3)	2326	(57.7)	1464	(33.7)
σw	3947	(4.6)	3819	(2.6)	3596	(4.4)
σwf	4154	(7.6)	3977	(6.4)	3763	(6.8)

(σ6) and a double minimum at 1.03 Å and 1.40 Å in βGal-H^+-H_2O (σ6′). In "pathological" cases such as these, VSCF predictions are known to be unreliable.

Ab Initio Molecular Dynamics Simulations. When AIMD methods are used to simulate molecular vibrational spectra, anharmonic effects are inherently included, and, in principle, they should remain reliable where the VSCF-PT2 method fails due to the "double well" character of the potential; they can also be used to simulate vibrational spectra at elevated temperatures. Accordingly, following the strategy outlined in section 2.4, the IR vibrational spectra of βGal-H^+ and βGal-H^+-H_2O were calculated using the CP2K package, at 40 and 300 K. They are shown in Figures 10 and 11, and the wavenumbers of the predicted vibrational modes are listed in Table 4, where they can be compared with the corresponding VSCF-PT2 predictions. Apart from the shared proton modes, σ6 in βGal-H^+ and σ6′ in βGal-H^+-H_2O, the simulations at low temperature (40 K) are in close accord with the VSCF data (within 40 cm^{-1}), which provides support for the reliability of the theoretical method, at least for the σ1−4 and the σw and

dx.doi.org/10.1021/jp3028325 | J. Phys. Chem. B 2012, 116, 4851−4859

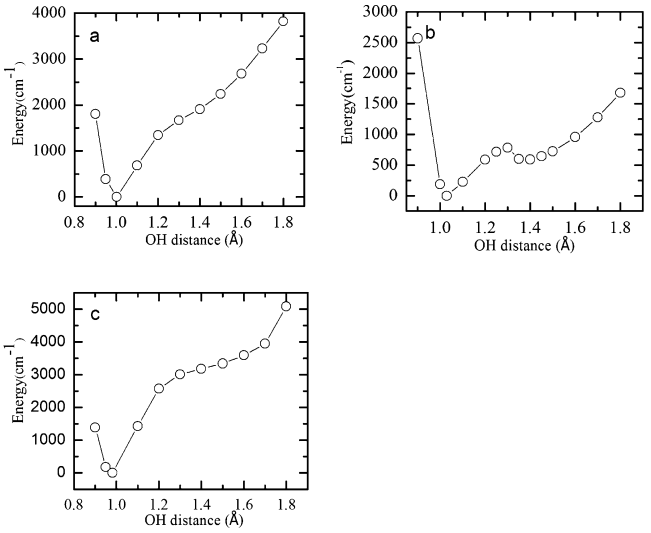

Figure 10. Scanned potentials of the OH bond in (a,c) β-D-galactose-H$^+$ (σ6 band and σ6′), and (b) β-D-galactose-H$^+$-H$_2$O (σ6′ band). To obtain each point in the figure, the OH band length was fixed in the calculation, and other coordinates were relaxed.

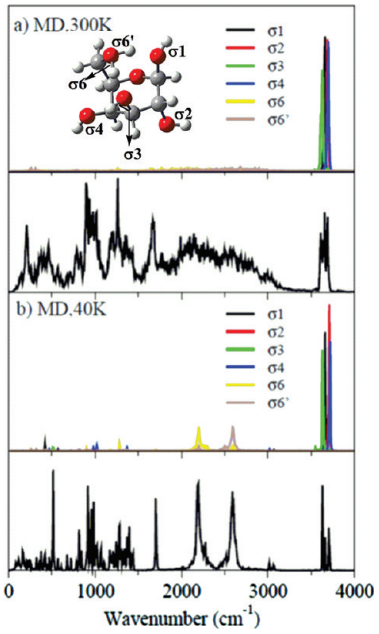

Figure 11. OH vibrational band assignments (top panels) and calculated IR spectra (lower panels) of β-D-galactose-H$^+$ at (a) 40 K and (b) 300 K.

σwf modes. The displacements in the "soft", shared proton modes, σ6 and σ6′ in βGal-H$^+$ and its hydrated complex, are now much smaller. In the latter case, the wavenumber σ6′ ~ 2085 cm^{-1}, predicted for the proton bound water complex, is similar to the observed wavenumber of the corresponding mode in the proton bound ethanol−water complex CH_3CH_2OH-H$^+$-H$_2$O,[49] which has a similar structure, with the proton moving between two O atom sites with similar proton affinities. In βGal-H$^+$, the large discrepancy between the frequency, σ6′, predicted by VSCF and the AIMD calculations is almost certainly due to breakdown of VSCF for this specific mode. As shown in Figure 10c, the σ6′ mode has a "shoulder" at energies relevant to the vibrational transition. The standard

Table 4. Comparisons between the Wavenumbers of OH Bands Calculated Using the VSCF Method (at 0 K) and through Ab Initio MD Simulations at 40 and 300 K

	β-D-galactose-H$^+$			β-D-galactose-H$^+$-H$_2$O		
		MD			MD	
mode	VSCF	40 K	300 K	VSCF	40 K	300 K
σ1	3668	3660	3660	3665	3690	3680
σ2	3675	3710	3690	3697	3690	3680
σ3	3651	3630	3630	3673	3670	3665
σ4	3683	3720	3700	3598	3610	3600
σ6	2004	2200	broad	2888	2825	broad
σ6′	2680	2590	broad	1464	2085	broad
σ_w				3596	3590	3600
σ_{wf}				3763	3750	3740

VSCF algorithm is inapplicable for such potentials. For the frequency σ6 in βGal-H$^+$-H$_2$O, the discrepancy between VSCF and AIMD is not very large (~60 cm^{-1}). We note that when the potential is not anomalous in form as above, VSCF is generally more accurate than AIMD, since it is a quantum-mechanical algorithm.

The AIMD simulations conducted at 300 K predict very little change in the wavenumbers of the high frequency OH modes in the two systems (see Figures 11 and 12 and Table 4), but the

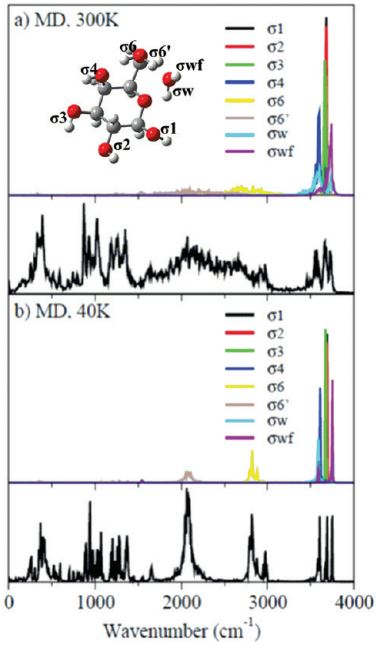

Figure 12. OH vibrational band assignments (top panels) and calculated IR spectra (lower panels) of β-D-galactose-H$^+$-H$_2$O at (a) 40 K and (b) 300 K.

softer, proton shared modes, σ6 and σ6′, become very broad due no doubt to large-amplitude motion (associated with proton transfer) at the elevated temperature. Their broadening is also evident from the band assignments, determined from the Fourier transform of the time dependence of the O−H bond lengths, which provide the vibrational band assignments shown in Figures 11 and 12.

dx.doi.org/10.1021/jp3028325 | J. Phys. Chem. B 2012, 116, 4851−4859

IV. CONCLUDING REMARKS

In the context of acid (or enzyme) catalyzed hydrolysis, the conformational structure, vibrational spectroscopy, and proton transfer dynamics in a protonated sugar, β-D-galactose-H^+, and its hydrated complex, β-D-galactose-H^+-H_2O, have been explored through ab initio calculations and AIMD simulations, conducted on-the-fly. They have led to the following main conclusions:

(1) The preferred site of protonation in both β-D-galactose-H^+ and its singly hydrated complex, is the oxygen atom, O6, in the hydroxymethyl group. The protonated ion adopts an inverted, $^1C_4$, conformation, which facilitates proton sharing with the neighboring atoms O1 and O3, now axially oriented.

(2) The OH vibrational modes associated with shared protons are strongly displaced toward low wavenumbers and reflect motions controlled by extended or double-well potentials.

(3) A reaction between the proton and the sugar, triggered by proton transfer from O6 to the anomeric atom, O1, can occur in β-D-galactose-H^+, on a time scale of <10 ps at 500 K, leading to the rupture of the C1−O1 bond, the elimination of H_2O, and the production of an oxacarbenium $[C_6H_{11}O_5]^+$ cation.

(4) In the hydrated complex, instead of providing a conduit for proton transfer from O6 to O1, followed by the formation of an oxacarbenium ion, the proton bound water molecule actually *blocks* the reactive pathway. Proton transfer can occur at 300 and 500 K, within 10 ps, but the positive charge is transferred to the bound water molecule, to create an H_3O^+ ion.

■ ASSOCIATED CONTENT

Supporting Information

The proton jump probability between two different O atoms in the β-D-galactose-H^+ and β-D-galactose-H^+-H_2O. This information is available free of charge via the Internet at http://pubs.acs.org/.

■ AUTHOR INFORMATION

Corresponding Author

*E-mail: hbxie@dlut.edu.cn (H.-b.X.); benny@fh.huji.ac.il (R.B.G.).

Notes

The authors declare no competing financial interest.

■ ACKNOWLEDGMENTS

We thank Dr. B. Brauer for her help with the VSCF calculations. We also thank the U.S. Department of Energy Office of Science (Grant DE-FG02-09ER64762) and the National Science Foundation (Grant CHE-0840513) for their support, and the NERSC for computational facilities and the expert assistance of their support staff. J.P.S. thanks the Leverhulme Trust for the award of an Emeritus Fellowship. H.-b. X. also thanks the support from "the Fundamental Research Funds for the Central Universities".

■ REFERENCES

(1) Blériot, Y.; Vadivel, S. K.; Herrera, A. J.; Greig, I. R.; Kirby, A. J.; Sinaÿ, P. *Tetrahedron* **2004**, *60*, 6813−6828.
(2) Davies, G. J.; Planas, A.; Rovira, C. *Acc. Chem. Res.* **2011**, *45*, 308−316.
(3) Qian, X. H.; Nimlos, M. R.; Johnson, D. K.; Himmel, M. E. *Appl. Biochem. Biotechnol.* **2005**, *121*, 989−997.
(4) Qian, X. H.; Nimlos, M. R.; Davis, M.; Johnson, D. K.; Himmel, M. E. *Carbohyd. Res.* **2005**, *340*, 2319−2327.
(5) Stubbs, J. M.; Marx, D. *Chem.—Eur. J.* **2005**, *11*, 2651−2659.
(6) Rudić, S.; Xie, H. B.; Gerber, R. B.; Simons, J. P. *Mol. Phys.* **2012**, in press.
(7) Li, X.; Moore, D. T.; Iyenagar, S. S. *J. Chem. Phys.* **2008**, *128*, 184308-1−184308-16.
(8) Brauer, B.; Pincu, M.; Buch, V.; Bar, I.; Simons, J. P.; Gerber, R. B. *J. Phys. Chem. A* **2011**, *115*, 5859−5872.
(9) Pincu, M.; Cocinero, E. J.; Mayorkas, N.; Brauer, B.; Davis, B. G.; Gerber, R. B.; Simons, J. P. *J. Phys. Chem. A* **2011**, *115*, 9498−9509.
(10) Jin, L.; Simons, J. P.; Gerber, R. B. *Chem. Phys. Lett.* **2011**, *518*, 49−54.
(11) Lelong, G.; Howells, W. S.; Brady, J. W.; Talon, C.; Price, D. L.; Saboungi, M. L. *J. Phys. Chem. B* **2009**, *113*, 13079−13085.
(12) Mason, P. E.; Neilson, G. W.; Enderby, J. E.; Saboungi, M. L.; Cuello, G.; Brady, J. W. *J. Chem. Phys.* **2006**, *125*, 224505-1−224505-9.
(13) Damm, W.; Frontera, A.; TiradoRives, J.; Jorgensen, W. L. *J. Comput. Chem.* **1997**, *18*, 1955−1970.
(14) Woods, R. J.; Fadda, E. *Drug. Discovery Today* **2010**, *15*, 596−609.
(15) Shemesh, D.; Chaban, G. M.; Gerber, R. B. *J. Phys. Chem. A* **2004**, *108*, 11477−11484.
(16) Shemesh, D.; Gerber, R. B. *J. Chem. Phys.* **2005**, *122*, 241104−241104−4.
(17) Shmilovitz-Ofir, M.; Gerber, R. B. *J. Am. Chem. Soc.* **2011**, *133*, 16510−16517.
(18) Pincu, M.; Brauer, B.; Gerber, R. B.; Buch, V. *Phys. Chem. Chem. Phys.* **2010**, *12*, 3550−3558.
(19) Marx, D.; Tuckerman, M. E.; Hutter, J.; Parrinello, M. *Nature* **1999**, *397*, 601−604.
(20) Mundy, C. J.; Kuo, I. F. W.; Tuckerman, M. E.; Lee, H. S.; Tobias, D. J. *Chem. Phys. Lett.* **2009**, *481*, 2−8.
(21) Pagliai, M.; Cavazzoni, C.; Cardini, G.; Erbacci, G.; Parrinello, M.; Schettino, V. *J. Chem. Phys.* **2008**, *128*, 224514-1−224514-7.
(22) Gaigeot, M. P. *Phys. Chem. Chem. Phys.* **2010**, *12*, 3336−3359.
(23) Momany, F. A.; Appell, M.; Willett, J. L.; Schnupf, U.; Bosma, W. B. *Carbohydr. Res.* **2006**, *341*, 525−537.
(24) Schmidt, M. W.; Baldridge, K. K.; Boatz, J. A.; Elbert, S. T.; Gordon, M. S.; Jensen, J. H.; Koseki, S.; Matsunaga, N.; Nguyen, K. A.; Su, S. J.; et al. *J. Comput. Chem.* **1993**, *14*, 1347−1363.
(25) Mohamadi, F.; Richards, N. G. J.; Guida, W. C.; Liskamp, R.; Lipton, M.; Caufield, C.; Chang, G.; Hendrikson, T.; Still, W. C. *J. Comput. Chem.* **1990**, *11*, 440−467.
(26) Frisch, M. J.; Trucks, G. W.; Schlegel, H. B.; Scuseria, G. E.; Robb, M. A.; Cheeseman, J. R.; Montgomery, Jr., J. A.; Vreven, T.; Kudin, K. N.; Burant, J. C. et al. *Gaussian 03*, revision B.03; Gaussian, Inc.: Pittsburgh, PA, 2003.
(27) Grimme, S. *J. Comput. Chem.* **2006**, *27*, 1787−1799.
(28) Grimme, S. *J. Comput. Chem.* **2004**, *25*, 1463−1473.
(29) Eichkorn, K.; Weigend, F.; Treutler, O.; Ahlrichs, R. *Theor. Chem. Acc.* **1997**, *97*, 119−124.
(30) Nose, S. *J. Chem. Phys.* **1984**, *81*, 511−519.
(31) Hoover, W. G. *Phys. Rev. A* **1985**, *31*, 1695−1697.
(32) Ahlrichs, R.; Bär, M.; Häser, M.; Horn, H.; Kölmel, C. *Chem. Phys. Lett.* **1989**, *162*, 165−169.
(33) Reed, A. E.; Weinstock, R. B.; Weinhold, F. *J. Chem. Phys.* **1985**, *83*, 735−746.
(34) Norris, L. S.; Ratner, M. A.; Roitberg, A. E.; Gerber, R. B. *J. Chem. Phys.* **1996**, *105*, 11261−11267.
(35) Chaban, G. M.; Jung, J. O.; Gerber, R. B. *J. Phys. Chem. A* **2000**, *104*, 10035−10044.
(36) Chaban, G. M.; Gerber, R. B. *J. Chem. Phys.* **2001**, *115*, 1340−1348.
(37) Gerber, R. B.; Chaban, G. M.; Gregurick, S. K.; Brauer, B. *Biopolymers* **2003**, *68*, 370.

(38) Adesokan, A. A.; Fredj, E.; Brown, E. C.; Gerber, R. B. *Mol. Phys.* **2005**, *103*, 1505−1520.
(39) Brauer, B.; Kabelac, M.; Hobza, P.; Bakker, J. M.; Riziq, A. G. A.; de Vries, M. S; Gerber, R. B. *J. Phys. Chem. A* **2005**, *109*, 6974−6984.
(40) Adesokan, A. A.; Pan, D. H.; Fredj, E.; Mathies, R. A.; Gerber, R. B. *J. Am. Chem. Soc.* **2007**, *129*, 4584−4594.
(41) Adesokan, A. A.; Chaban, G. M.; Dopfer, O.; Gerber, R. B. *J. Phys. Chem. A* **2007**, *111*, 7374−7381.
(42) Adesokan, A. A.; Gerber, R. B. *J. Phys. Chem. A* **2009**, *113*, 1905−1912.
(43) McQuarrie, D. A. *Statistical Mechanics*; Harper-Collins: New York, 1976.
(44) Car, R.; Parrinello, M. *Phys. Rev. Lett.* **1985**, *55*, 2471−2474.
(45) Grimme, S.; Antony, J.; Ehrlich, S.; Krieg, H. *J. Chem. Phys.* **2010**, *132*, 154104-1−154104-19.
(46) Goedecker, S.; Teter, M.; Hutter, J. *Phys. Rev. B* **1996**, *54*, 1703−1710.
(47) Bernasconi, M.; Silvestrelli, P. L.; Parrinello, M. *Phys. Rev. Lett.* **1998**, *81*, 1235−1238.
(48) Wang, F. F.; Jenness, G.; Al-Saidi, W. A.; Jordan, K. D. *J. Chem. Phys.* **2010**, *132*, 134303-1−134303-8.
(49) Roscioli, J. R.; McCunn, L. R.; Johnson, M. A. *Science* **2007**, *316*, 249−254.
(50) Vendrell, O.; Meyer, H. D. *Phys. Chem. Chem. Phys.* **2008**, *10*, 4692−4703.
(51) McCoy, A. B.; Huang, X. C.; Carter, S.; Landeweer, M. Y.; Bowman, J. M. *J. Chem. Phys.* **2005**, *122*, 061101-1−061101-4.
(52) Kaledin, M.; Kaledin, A. L.; Bowman, J. M. *J. Phys. Chem. A* **2006**, *110*, 2933−2939.
(53) Huang, X. C.; Braams, B. J.; Bowman, J. M. *J. Chem. Phys.* **2005**, *122*, 044308-1−044308-12.
(54) Hammer, N. I.; Diken, E. G.; Roscioli, J. R.; Johnson, M. A.; Myshakin, E. M.; Jordan, K. D.; McCoy, A. B.; Huang, X.; Bowman, J. M.; Carter, S. *J. Chem. Phys.* **2005**, *122*, 244301-1−244301-10.
(55) Diken, E. G.; Headrick, J. M.; Roscioli, J. R.; Bopp, J. C.; Johnson, M. A.; McCoy, A. B. *J. Phys. Chem. A* **2005**, *109*, 1487−1490.
(56) Qian, X. H. *Abstr. Pap. Am. Chem. Soc.* **2005**, *229*, U862.
(57) Simons, J. P.; Jockusch, R. A.; Carcabal, P.; Hung, I.; Kroemer, R. T.; Macleod, N. A.; Snoek, L. C. *Int. Rev. Phys. Chem.* **2005**, *24*, 489−531.
(58) Gerber, R. B.; Chaban, G. M.; Brauer, B.; Miller, Y., *First principles Calculations of Anharmonic Vibrational Spectroscopy of Large Molecules in Theory and Applications of Computational Chemistry: The First 40 Years*; Dykstra, C. E., Frenking, G., Kim, K. S., Scuseria, G. E., Eds.; Elsevier: Holland, 2005; Chapter 9, pp 165−193.